Topological edge states and Aharanov-Bohm caging with ultracold atoms carrying orbital angular momentum

G. Pelegrí,[1] A. M. Marques,[2] R. G. Dias,[2] A. J. Daley,[3] J. Mompart,[1] and V. Ahufinger[1]
[1]*Departament de Física, Universitat Autònoma de Barcelona, E-08193 Bellaterra, Spain*
[2]*Department of Physics and I3N, University of Aveiro, 3810-193 Aveiro, Portugal*
[3]*Department of Physics and SUPA, University of Strathclyde, Glasgow G4 0NG, United Kingdom*

(Received 11 July 2018; published 11 February 2019)

We show that bosonic atoms loaded into orbital angular momentum $l = 1$ states of a lattice in a diamond-chain geometry provide a flexible and simple platform for exploring a range of topological effects. This system exhibits robust edge states that persist across the gap-closing points, indicating the absence of a topological transition. We discuss how to perform the topological characterization of the model with a generalization of the Zak's phase and we show that this system constitutes a realization of a square-root topological insulator. Furthermore, the relative phases arising naturally in the tunneling amplitudes lead to the appearance of Aharanov-Bohm caging in the lattice. We discuss how these properties can be realized and observed in ongoing experiments.

DOI: 10.1103/PhysRevA.99.023613

I. INTRODUCTION

Topological properties play an important role in a wide range of condensed matter systems [1]. Such properties are particularly demonstrated by topological insulators [2], where a bulk-boundary correspondence correlates the nontrivial topological indices of the bulk energy bands such as the Berry phase [3], with the existence of topological edge states under open boundary conditions. The importance of these concepts has led to a great deal of interest in finding clean environments in which fundamental features of the system can be observed, and phenomena arising from interactions and nonequilibrium dynamical effects can be explored. Highlights of this include the realization of the Haldane [4] and Hofstadter [5,6] models with ultracold atoms, as well as the experimental measurement [7] of Zak's phase [8] and the detection of topological states [9,10], which complements parallel work in photonic waveguides [11–17]. There are a wide range of further theoretical proposals for observation of topological phenomena in cold atoms [18–25], most of which are based around the realization of artificial gauge fields by laser dressing [5,6,26], or periodically driving the lattice system [27].

Here, we explore topologically nontrivial multilevel models that arise naturally for ultracold atoms in excited orbital angular momentum (OAM) states of a one-dimensional (1D) chain. We study a concrete example of a diamond chain to demonstrate how this model is rendered topologically nontrivial due to relative phases in tunneling amplitudes for different OAM states. Remarkably, we find that topological states exist regardless of the values of the parameters of the model, with no topological transition across the gap-closing points. This system constitutes an unusual example of a topological insulator with nonquantized values of the Zak's phase due to the inversion axes not crossing the center of any choice of unit cell [8], and we make use of recently developed techniques [28] to perform the topological characterization. Furthermore, the model belongs to a new class of square-root topological insulators [29,30], in which the quantized values of the Zak's phases are recovered after taking the square of the bulk Hamiltonian.

Fundamentally, this behavior arises because the local OAM $l = 1$ states are equivalent to the p_x and p_y orbitals in optical lattices, which have been shown to naturally display nontrivial topological properties in one- [31] and two- [32,33] dimensional systems due to the parity of their wave functions. In the OAM $l = 1$ basis, the mechanism that yields topological properties is the appearance of relative phases in the tunneling amplitudes, which are controllable by tuning the geometry of the lattice [34]. We show that this can be observed directly in the corresponding experiments.

Additionally, a proper tuning of the intersite separation and the central angle can lead to Aharonov-Bohm (AB) caging [35,36]. A distinctive advantage regarding the realization of AB caging in this model, in relation to other proposals [30,37–39], is that one does not need to rely on creating synthetic gauge fields [40–43] to produce the magnetic flux required for AB caging. Instead, in our OAM $l = 1$ model complex phases with values controlled by the central angle appear naturally at some of the tunneling parameters [34,44], giving rise to an effective magnetic flux.

The rest of the paper is organized as follows. In Sec. II, we present the physical system and we discuss its basic properties and symmetries. In Sec. III, we present a series of analytical mappings that allow to gain insight into the system and to perform its topological characterization. In Sec. IV, we support the analytical findings discussed in the previous section with numerical results and we discuss under which conditions and to which extent the system exhibits AB caging. In Sec. V, we make some considerations regarding the experimental implementation of the diamond chain loaded with bosons in the OAM $l = 1$ states. Finally, in Sec. VI we briefly summarize the main conclusions of this work.

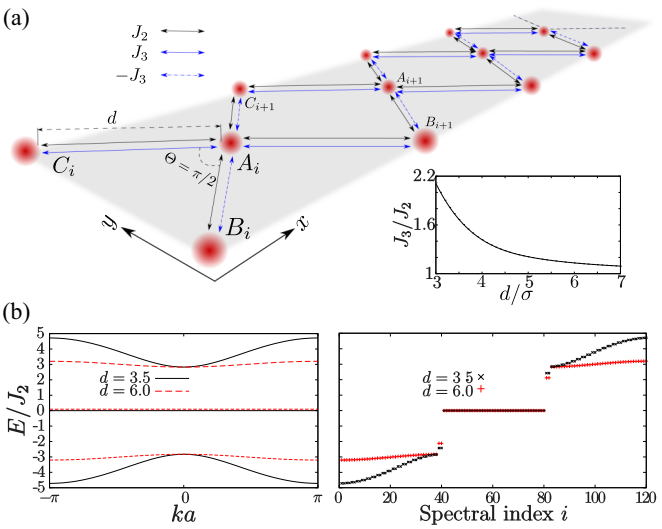

FIG. 1. (a) Schematic representation of the considered diamond chain. The inset shows, for harmonic oscillator traps, the dependence of the relative value of J_2 and J_3 on the intersite separation d, expressed in units of $\sigma = \sqrt{\hbar/(m\omega)}$. (b) Energy spectrum of the diamond chain with OAM $l = 1$ states. The left plot shows the band structure computed for $d = 3.5\sigma$, corresponding to $J_3/J_2 = 1.67$ (black solid line) and $d = 6\sigma$, corresponding to $J_3/J_2 = 1.13$ (red dotted line). In the right plot, the corresponding exact diagonalization spectra of a diamond chain of $N_c = 20$ unit cells are shown.

II. PHYSICAL SYSTEM

We consider a quasi-one-dimensional optical lattice with a diamond-chain shape. As shown in Fig. 1(a), the unit cells of this chain, labeled with the index i, are formed of three sites A_i, B_i, and C_i, each corresponding to a cylindrically symmetric potential of radial frequency ω, and forming a triangle with central angle $\Theta = \pi/2$ and nearest-neighbor separation d. We assume that the lattice is composed of an integer number N_c of unit cells, so that its right termination has a closed edge. The chain is loaded with noninteracting ultracold atoms of mass m that may occupy the two degenerate OAM $l = 1$ states with positive or negative circulation localized at each site, $\langle \vec{r}|j_i, \pm\rangle = \psi(r_{j_i})e^{\pm i(\varphi_{j_i}-\varphi_0)}$, where $j \in \{A, B, C\}$, (r_{j_i}, φ_{j_i}) are the polar coordinates with origin at the site j_i, and φ_0 is the phase origin. The tunneling dynamics of this type of states has been studied in detail in [34]. Between two neighboring sites, there are only three independent tunneling amplitudes: J_1, which corresponds to the self-coupling at each site between the two OAM states with different circulations, and J_2 and J_3, which correspond to the cross coupling between OAM states in different sites with equal or different circulations, respectively. The tunneling amplitudes between states with different OAM circulations J_1 and J_3 acquire relative phases that depend on φ_0, which is determined by Θ in the diamond-chain lattice. For $\Theta = \pi/2$, due to destructive interference between neighboring sites with different phases in the tunneling amplitudes, the self-coupling vanishes everywhere except for the sites at the left edges B_1 and C_1. Moreover, since typically $|J_1| \ll |J_2|, |J_3|$ [34], in this paper we neglect the self-coupling term at these two sites and leave a study of its consequences for Ref. [45]. Choosing φ_0 to point along the direction of the line that connects the sites C_i, A_i, and B_{i+1} and assuming coupling only between nearest-neighboring sites due to the rapid decay of the tunneling amplitudes as the intersite separation increases [45], the noninteracting Hamiltonian of the system takes the form ($\hbar \equiv 1$)

$$\hat{H} = J_2 \sum_{i=1}^{N_c} \sum_{\alpha=\pm} \left[\hat{a}_\alpha^{i\dagger}\left(\hat{b}_\alpha^i + \hat{b}_\alpha^{i+1} + \hat{c}_\alpha^i + \hat{c}_\alpha^{i+1}\right)\right] + J_3 \sum_{i=1}^{N_c} \sum_{\alpha=\pm} \left[\hat{a}_\alpha^{i\dagger}\left(e^{-2\alpha i\Theta}\hat{b}_{-\alpha}^i + \hat{b}_{-\alpha}^{i+1} + \hat{c}_{-\alpha}^i + e^{-2\alpha i\Theta}\hat{c}_{-\alpha}^{i+1}\right)\right] + \text{H.c.} \quad (1)$$

In our convention for φ_0, we see that a π phase is acquired in tunneling $B_i \leftrightarrow A_i \leftrightarrow C_{i+1}$ for a central angle $\Theta = \pi/2$. As shown in the inset of Fig. 1(a), the relative value of J_2 and J_3 depends on the intersite separation d, starting at $J_3/J_2 \approx 2.2$ for $d = 3\sigma$ and tending rapidly and asymptotically to $J_3/J_2 = 1$ as d increases. The diamond lattice with two states per site described by (1) possesses inversion symmetry, leading to a quantization to 0 or π (mod 2π) of the Zak's phases [8]. Additionally, since the model is bipartite it has chiral symmetry defined as $\Gamma\hat{H}\Gamma = -\hat{H}$, which entails that the energy spectrum is symmetric around 0.

By applying a series of exact mappings, we shall demonstrate that these symmetries are accompanied by the presence of topologically protected states localized at the right edge of the chain. Under periodic boundary conditions, the bulk Hamiltonian corresponding to the Fourier transform of (1) yields six energy bands after diagonalization. Their dispersion relations appear in three degenerate pairs $E(k) = 0, \pm 2\sqrt{(J_2^2 + J_3^2) + \cos(ka)(J_2^2 - J_3^2)}$, where $a = \sqrt{2}d$ is the lattice constant. The band structure presents a gap of size $2\sqrt{2}J_2$ (for $J_3 > J_2$) or $2\sqrt{2}J_3$ (for $J_3 < J_2$) and, in the $J_2 = J_3$ limit, all bands become flat. As shown in the energy spectrum of Fig. 1(b), for an experimentally feasible intersite separation of $d = 6\sigma$, one is already very close to this all-flat limit. In the case of open boundary conditions, exact diagonalization performed for a chain with $N_c = 20$ unit cells, shown in Fig. 1(b), reveals the presence of four in-gap states localized at the right edge of the chain. Importantly, these in-gap states persist provided both J_2 and J_3 are nonzero, implying that there is no topological transition across the gap-closing points.

III. ANALYTICAL MAPPINGS

The twofold degeneracy of the spectrum and the presence of gaps in the band structure can be understood by performing a rotation into a basis of symmetric and antisymmetric states $|D_i, \pm\rangle = \frac{1}{\sqrt{2}}(|C_i, +\rangle \pm |B_i, +\rangle)$, $|F_i, \pm\rangle = \frac{1}{\sqrt{2}}(|C_i, -\rangle \pm |B_i, -\rangle)$. This rotation decouples the diamond chain with six states per unit cell (1) into two independent and identical diamond chains H^+ and H^-, which have three states per unit cell [see Fig. 2(a)]. These two chains are described by

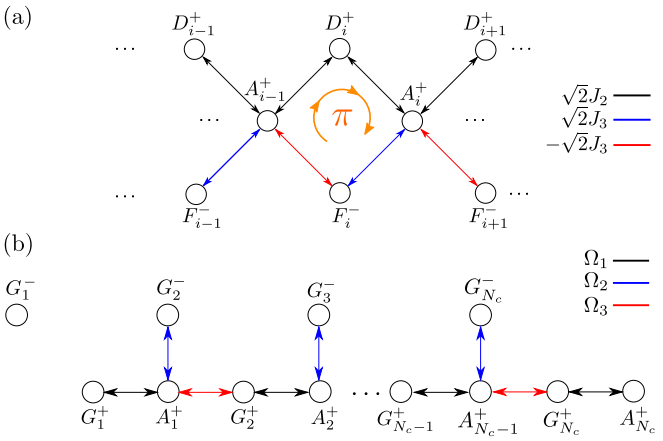

FIG. 2. Schematic representation of the tight-binding models obtained through the different mappings. (a) H^+ diamond chain obtained after applying the basis rotation $\{|B_i,\pm\rangle, |C_i,\pm\rangle\} \to \{|F_i,\pm\rangle, |D_i,\pm\rangle\}$ to the original OAM $l=1$ diamond chain. (b) Modified SSH model obtained after applying the basis rotation $\{|D_i,+\rangle, |F_i,-\rangle\} \to \{|G_i,\pm\rangle\}$ to the H^+ chain. N_c is the total number of unit cells.

the Hamiltonians

$$\hat{H}^+ = \sum_{i=1}^{N_c} \hat{a}^{i\dagger}_+ [\sqrt{2}J_2(\hat{d}^i_+ + \hat{d}^{i+1}_+) + \sqrt{2}J_3(\hat{f}^i_- - \hat{f}^{i+1}_-)] + \text{H.c.}, \tag{2a}$$

$$\hat{H}^- = \sum_{i=1}^{N_c} \hat{a}^{i\dagger}_- [\sqrt{2}J_2(\hat{f}^i_+ + \hat{f}^{i+1}_+) + \sqrt{2}J_3(\hat{d}^i_- - \hat{d}^{i+1}_-)] + \text{H.c.} \tag{2b}$$

The minus sign in one of the couplings can be associated with a net π flux through the plaquettes of these diamond chains [45], which explains the gap in the band structure [46]. Furthermore, the existence of in-gap edge states and the flattening of the bands in the $J_2 = J_3$ limit can be understood by means of a second basis rotation for each of the two subchains H^+ and H^-. For the H^+ chain, this basis rotation is given by $|G_i,+\rangle = \frac{1}{\sqrt{J_2^2+J_3^2}}(J_2|D_i,+\rangle + J_3|F_i,-\rangle)$ and $|G_i,-\rangle = \frac{1}{\sqrt{J_2^2+J_3^2}}(J_3|D_i,+\rangle - J_2|F_i,-\rangle)$. An equivalent rotation can be defined for the H^- chain by replacing $F \leftrightarrow D$. After applying this transformation, the H^+ diamond chain is mapped into a modified Su-Schrieffer-Heeger (SSH) model [47] with an extra dangling state per unit cell, as shown in Fig. 2(b), which is described by the Hamiltonian

$$\hat{H}^+_{\text{SSH}} = \sum_{i=1}^{N_c} \hat{a}^{i\dagger}_+ (\Omega_1 \hat{g}^i_+ + \Omega_2 \hat{g}^{i+1}_- + \Omega_3 \hat{g}^{i+1}_+) + \text{H.c.}, \tag{3}$$

where $\Omega_1 = \sqrt{2}\sqrt{J_2^2+J_3^2}$ and $\Omega_3 = \frac{\sqrt{2}(J_2^2-J_3^2)}{\sqrt{J_2^2+J_3^2}}$ are the strong and weak horizontal couplings and $\Omega_2 = \frac{2\sqrt{2}J_2J_3}{\sqrt{J_2^2+J_3^2}}$ is the coupling strength of the dangling state of each unit cell i to the central state $|A_i,+\rangle$. From Eq. (3), a compact expression for the zero-energy flat band states $\hat{H}^+_{\text{SSH}}|0\rangle^+_i = 0$ can be derived:

$$|0\rangle^+_i = \frac{1}{\sqrt{C}}\left(\frac{\Omega_3}{\Omega_2}|G_i,-\rangle - |G_i,+\rangle + \frac{\Omega_1}{\Omega_2}|G_{i+1},-\rangle\right). \tag{4}$$

In the original basis $\{|j_i,\pm\rangle\}$, the most localized forms of the zero-energy states (4) span the four sites surrounding the central site A_i, with no contribution from the states at this site. Additionally, $|G_1,-\rangle$ is a completely decoupled zero-energy state localized at the left edge of the chain [see Fig. 2(b)]. In the $J_2 = J_3$ limit, we have $\Omega_3 = 0$ and the bulk of the chain can be decomposed into isolated trimers $\{|G_i,+\rangle, |A_i,+\rangle, |G_{i+1},-\rangle\}$ with equal internal couplings $\Omega_1 = \Omega_2 = 2J_2$. The eigenstates of these trimers with a component of the state $|A_i,+\rangle$ are the top and bottom flat-band states $|E\pm\rangle^+_i$:

$$|E\pm\rangle^+_i = \frac{1}{2}(|G_i,+\rangle \pm \sqrt{2}|A_i,+\rangle + |G_{i+1},-\rangle);$$
$$\hat{H}^+_{\text{SSH}}|_{\Omega_3=0}|E\pm\rangle^+_i = \pm 2\sqrt{2}J_2|E\pm\rangle^+_i. \tag{5}$$

However, at the right edge of the chain there is a dimer formed by the states $|G_{N_c},+\rangle$ and $|A_{N_c},+\rangle$, whose eigenstates $|\text{Edge},\pm\rangle^+$ have the following expressions and energies:

$$|\text{Edge}\pm\rangle^+ = \frac{1}{\sqrt{2}}(|G_{N_c},+\rangle \pm |A_{N_c},+\rangle);$$
$$\hat{H}^+_{\text{SSH}}|_{\Omega_3=0}|\text{Edge}\pm\rangle^+ = \pm 2J_2|\text{Edge}\pm\rangle^+. \tag{6}$$

As shown in Fig. 1(b), in-gap states appear also for general values of the couplings $J_2 \neq J_3$. In this scenario, these states are strongly localized at the right edge of the chain, exhibiting an exponentially decaying tail to the bulk, which widens as one deviates from the $J_2 = J_3$ limit [45]. In order to tell whether this robustness is due to topological effects, one should compute the Zak's phase for each band, which are the relevant quantities to topologically characterize one-dimensional models [8]. However, the computation of the Zak's phases is not straightforward in our system. In the original OAM $l = 1$ model (1) the degeneracy of the bands means that their Zak's phases are ill defined. On the other hand, each of the decoupled chains of the two successive mappings given by the Hamiltonians in (2) and (3), respectively, does not have inversion symmetry, so that the Zak's phase can yield nonquantized values. In order to circumvent these limitations, a third mapping can be introduced, through a basis rotation of (3) (see [45] for details), wherein inversion symmetry and, therefore, a quantized Zak's phase for each band is recovered. Under this third mapping, the system becomes a diamond chain with alternating tunneling amplitudes, whose nontrivial topological nature of the gaps where the edge states lie is explicitly shown in [48], making use of the technique described in [28] to circumvent the fact that the inversion axes do not cross the center of any choice of the unit cell. As stated above, a striking feature of the topology of this model, directly carried over to the original OAM $l = 1$ model, is that there is no topological transition across the gap-closing point, as can be seen by fixing either J_2 or J_3 and varying the other across zero. We find that this model constitutes a realization of a square-root topological insulator using ultracold atoms

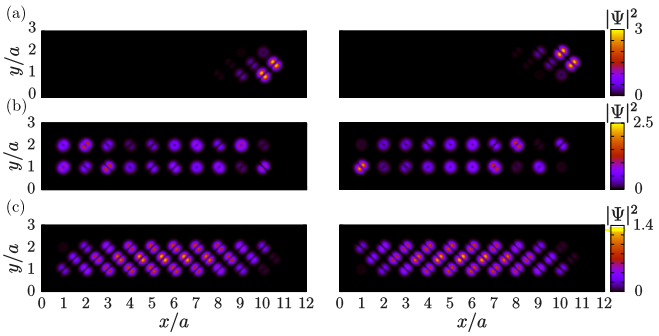

FIG. 3. Density profiles of numerically obtained eigenstates for a diamond chain of $N_c = 10$ units cells and intersite separation $d = 6\sigma$, corresponding to $J_3/J_2 = 1.13$. (a) Two degenerate edge states. (b) Two states of the flat band. (c) The two degenerate ground states.

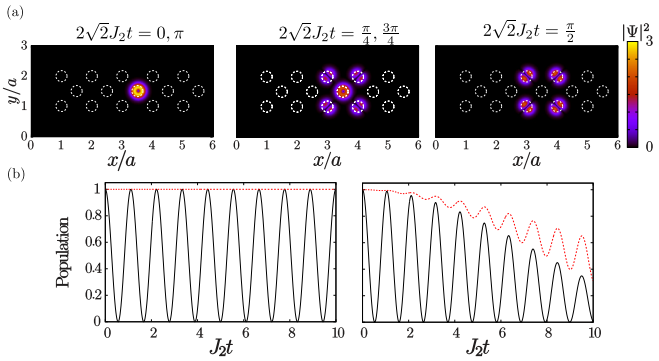

FIG. 4. AB caging in a diamond chain of $N_c = 5$ unit cells. (a) Snapshots at different times of the density profiles corresponding to the time evolution of a wave packet initially prepared in the state $|A_3, +\rangle$ in the perfect caging limit $J_2/J_3 = 1$. (b) Time evolution of the population of the same initial state as in (a) (black solid lines) and the total population of the cage (red dotted lines) for $J_3/J_2 = 1$ (left panel) and 1.1 (right panel).

[45] like the one recently reported in a photonic system [30]. In this type of topological insulator, the usual expression of the Zak's phase $\gamma_n = -i \int_k^{k+2\pi} dk \, \langle u_n(k)| \frac{d}{dk} |u_n(k)\rangle$ yields nonquantized values, but by squaring the bulk Hamiltonian, centered inversion axes within the unit cell and quantized Zak's phases are recovered.

IV. NUMERICAL RESULTS

To illustrate these results, in Fig. 3 we show the numerical density plots of the different types of states that can be found in a diamond chain of $N_c = 10$ unit cells and a separation between nearest-neighbor sites $d = 6\sigma$, corresponding to $J_3/J_2 = 1.13$. In Fig. 3(a), two degenerate edge states are shown, evidencing their strong localization at the right end of the chain. In Fig. 3(b), two examples of zero-energy states, which have no population at the central (A) sites of the chain, are displayed. These contain components of many maximally localized states (4) and, in the case of the state at the right panel, also of the zero-energy decoupled mode localized at the left edge $|G_1, -\rangle$ [see Fig. 2(b)]. Finally, Fig. 3(c) shows the two degenerate ground states of the system. In Figs. 3(a) and 3(c), the states at the left and right panels have different orientations of the nodal lines due to the fact that they belong to the two different subchains H^+ and H^-.

Aharanov-Bohm caging

Finally, we show that in the $J_2 = J_3$ limit the system can exhibit AB caging. In this limit, from the relations (5) and the equivalent ones for the H^- chain, we can express the states $|A_i, \pm\rangle$ in terms of flat-band states that occupy solely the four sites surrounding A_i, i.e., B_i, B_{i+1}, C_i, and C_{i+1}. Therefore, an initial state prepared in an arbitrary superposition of the $|A_i, +\rangle$ and $|A_i, -\rangle$ states will oscillate coherently to its four neighboring sites with a frequency $\omega = 2\sqrt{2}J_2$ (given by the absolute value of the energies of the top and bottom flat-band states) and, therefore, never leave the cage formed by the unit cells i and $i+1$. In Fig. 4(a), we show some snapshots of the time evolution of a wave packet prepared initially in the state $|A_3, +\rangle$ of a diamond chain with $N_c = 5$ unit cells. In a real experiment, the condition $J_2 = J_3$ would never be exactly fulfilled, but for sufficiently close values the AB caging would persist for a significant amount of time. In Fig. 4(b), we plot, for the same initial state as in Fig. 4(a), the time evolution of the population of the state $|A_3, +\rangle$ and the total sum of the states forming the cage for $J_3/J_2 = 1, 1.1$ (left and right panels, respectively). While perfect caging only occurs for $J_3/J_2 = 1$, for $J_3/J_2 = 1.1$ we observe that approximately 40% of the population remains on the cage after a time $J_2t = 10$.

V. EXPERIMENTAL IMPLEMENTATION

An optical diamond chain could be implemented by using two pairs of counterpropagating lasers at $\pm 45^\circ$ with respect to the x axis in a quasi-1D cigar-shape geometry [49]. To load atoms in the OAM $l = 1$ manifold of local sites of the lattice, which are combinations of the p-band orbitals of the form $p_x \pm ip_y$ [50,51], three different approaches could be used: to adiabatically modify the trapping potentials such that atoms are transferred from the ground to the p band of an adjacent well via resonant tunneling [52], to combine lattice shaking with shortcuts to adiabaticity to promote the atoms to the p band [53], and, finally, to directly transfer OAM from a light beam to the trapped atoms [54]. Once the atoms are loaded into the p band, loss of population can be induced by collisions that transfer one atom to the lowest band, and one to a higher band. This is strongly suppressed for dilute samples and weak interactions, and in deep lattices where bandwidths are small anharmonicity ensures that the process is not resonant. To detect the atomic distribution and thereby AB caging and edge states with single-site resolution in the diamond chain, the quantum gas microscope technique [55,56] could be used. This technique has recently been applied to observe topological states of ultracold bosonic atoms in optical lattices [57,58]. On the other hand, edge states have been observed with an atomic Bose gas in the quantum Hall regime [59] making use of the synthetic dimensions provided by the internal degrees of freedom.

VI. CONCLUSIONS

In summary, OAM provides phases in the tunneling amplitudes, which can be tuned by modifying the geometry. For realistic experimental parameters, this can be used to directly observe topological edge states and AB caging in a diamond chain. This could form the basis for future studies of interacting particles, and also a broad range of scenarios of out-of-equilibrium dynamics in topological lattices.

ACKNOWLEDGMENTS

G.P., J.M., and V.A. gratefully acknowledge financial support from the Ministerio de Economía y Competitividad, MINECO (FIS2014-57460-P, FIS2017-86530-P) and from the Generalitat de Catalunya (SGR2017-1646). G.P. acknowledges financial support from MINECO through Grant No. BES-2015-073772. A.M.M. acknowledges financial support from the Portuguese Institute for Nanostructures, Nanomodelling and Nanofabrication (i3N) through the Grant No. BI/UI96/6376/2018. A.M.M. and R.G.D. acknowledge funding by the FEDER funds through the COMPETE 2020 Programme and National Funds throught FCT-Portuguese Foundation for Science and Technology under the Project No. UID/CTM/50025/2013 and under the Project No. PTDC/FIS-MAC/29291/2017. Work at the University of Strathclyde was supported by the EPSRC Programme Grant DesOEQ (No. EP/P009565/1). We thank A. Celi, A. Dauphin, A. Buyskikh, and S. Flannigan for helpful discussions.

[1] X.-L. Qi and S.-C. Zhang, Rev. Mod. Phys. **83**, 1057 (2011).
[2] M. Z. Hasan and C. L. Kane, Rev. Mod. Phys. **82**, 3045 (2010).
[3] M. V. Berry, Proc. R. Soc. London, Ser. A **392**, 45 (1984).
[4] G. Jotzu, M. Messer, R. Desbuquois, M. Lebrat, T. Uehlinger, D. Greif, and T. Esslinger, Nature (London) **515**, 237 (2014).
[5] M. Aidelsburger, M. Atala, M. Lohse, J. T. Barreiro, B. Paredes, and I. Bloch, Phys. Rev. Lett. **111**, 185301 (2013).
[6] H. Miyake, G. A. Siviloglou, C. J. Kennedy, W. C. Burton, and W. Ketterle, Phys. Rev. Lett. **111**, 185302 (2013).
[7] M. Atala, M. Aidelsburger, J. T. Barreiro, D. Abanin, T. Kitagawa, E. Demler, and I. Bloch, Nat. Phys. **9**, 795 (2013).
[8] J. Zak, Phys. Rev. Lett. **62**, 2747 (1989).
[9] M. Leder, C. Grossert, L. Sitta, M. Genske, A. Rosch, and M. Weitz, Nat. Commun. **7**, 13112 (2016).
[10] E. J. Meier, F. A. An, and B. Gadway, Nat. Commun. **7**, 13986 (2016).
[11] Y. E. Kraus, Y. Lahini, Z. Ringel, M. Verbin, and O. Zilberberg, Phys. Rev. Lett. **109**, 106402 (2012).
[12] M. Verbin, O. Zilberberg, Y. E. Kraus, Y. Lahini, and Y. Silberberg, Phys. Rev. Lett. **110**, 076403 (2013).
[13] M. Hafezi, S. Mittal, J. Fan, A. Migdall, and J. M. Taylor, Nat. Photon. **7**, 1001 (2013).
[14] P. St-Jean, V. Goblot, E. Galopin, A. Lemaître, T. Ozawa, L. Le Gratiet, I. Sagnes, J. Bloch, and A. Amo, Nat. Photon. **11**, 651 (2017).
[15] S. Weimann, M. Kremer, Y. Plotnik, Y. Lumer, S. Nolte, K. G. Makris, M. Segev, M. C. Rechtsman, and A. Szameit, Nat. Mater. **16**, 433 (2017).
[16] T. Kitagawa, M. A. Broome, A. Fedrizzi, M. S. Rudner, E. Berg, I. Kassal, A. Aspuru-Guzik, E. Demler, and A. G. White, Nat. Commun. **3**, 882 (2012).
[17] F. Cardano, A. D'Errico, A. Dauphin, M. Maffei, B. Piccirillo, C. de Lisio, G. De Filippis, V. Cataudella, E. Santamato, L. Marrucci, M. Lewenstein, and P. Massignan, Nat. Commun. **8**, 15516 (2017).
[18] N. Goldman, J. C. Budich, and P. Zoller, Nat. Phys. **12**, 639 (2016).
[19] M. Metcalf, C.-Y. Lai, K. Wright, and C.-C. Chien, Europhys. Lett. **118**, 56004 (2017).
[20] S. Mugel, A. Celi, P. Massignan, J. K. Asbóth, M. Lewenstein, and C. Lobo, Phys. Rev. A **94**, 023631 (2016).
[21] H. Nonne, M. Moliner, S. Capponi, P. Lecheminant, and K. Totsuka, Europhys. Lett. **102**, 37008 (2013).
[22] X.-J. Liu, Z.-X. Liu, and M. Cheng, Phys. Rev. Lett. **110**, 076401 (2013).
[23] M. Nakagawa and N. Kawakami, Phys. Rev. B **96**, 155133 (2017).
[24] F. Matsuda, M. Tezuka, and N. Kawakami, J. Phys. Soc. Jpn. **83**, 083707 (2014).
[25] X. Deng and L. Santos, Phys. Rev. A **89**, 033632 (2014).
[26] D. Jaksch and P. Zoller, New J. Phys. **5**, 56 (2003).
[27] K. Jiménez-García, L. J. LeBlanc, R. A. Williams, M. C. Beeler, A. R. Perry, and I. B. Spielman, Phys. Rev. Lett. **108**, 225303 (2012).
[28] A. M. Marques and R. G. Dias, arXiv:1707.06162 [cond-mat.mes-hall].
[29] J. Arkinstall, M. H. Teimourpour, L. Feng, R. El-Ganainy, and H. Schomerus, Phys. Rev. B **95**, 165109 (2017).
[30] M. Kremer, I. Petrides, E. Meyer, M. Heinrich, O. Zilberberg, and A. Szameit, arXiv:1805.05209.
[31] X. Li, E. Zhao, and W. Vincent Liu, Nat. Commun. **4**, 1523 (2013).
[32] K. Sun, W. V. Liu, A. Hemmerich, and S. Das Sarma, Nat. Phys. **8**, 67 (2012).
[33] Z.-F. Xu, L. You, A. Hemmerich, and W. V. Liu, Phys. Rev. Lett. **117**, 085301 (2016).
[34] J. Polo, J. Mompart, and V. Ahufinger, Phys. Rev. A **93**, 033613 (2016).
[35] J. Vidal, R. Mosseri, and B. Douçot, Phys. Rev. Lett. **81**, 5888 (1998).
[36] B. Douçot and J. Vidal, Phys. Rev. Lett. **88**, 227005 (2002).
[37] J. Jünemann, A. Piga, S.-J. Ran, M. Lewenstein, M. Rizzi, and A. Bermudez, Phys. Rev. X **7**, 031057 (2017).
[38] S. Longhi, Opt. Lett. **39**, 5892 (2014).
[39] S. Mukherjee, M. Di Liberto, P. Öhberg, R. R. Thomson, and N. Goldman, Phys. Rev. Lett. **121**, 075502 (2018).
[40] J. Dalibard, F. Gerbier, G. Juzeliūnas, and P. Öhberg, Rev. Mod. Phys. **83**, 1523 (2011).
[41] N. Goldman, G. Juzeliūnas, P. Öhberg, and I. B. Spielman, Rep. Prog. Phys. **77**, 126401 (2014).
[42] N. Goldman and J. Dalibard, Phys. Rev. X **4**, 031027 (2014).
[43] M. Aidelsburger, S. Nascimbene, and N. Goldman, C. R. Physique **19**, 394 (2018).

[44] G. Pelegrí, J. Polo, A. Turpin, M. Lewenstein, J. Mompart, and V. Ahufinger, Phys. Rev. A **95**, 013614 (2017).
[45] G. Pelegrí, A. M. Marques, R. G. Dias, A. J. Daley, V. Ahufinger, and J. Mompart, Phys. Rev. A **99**, 023612 (2019).
[46] A. A. Lopes and R. G. Dias, Phys. Rev. B **84**, 085124 (2011).
[47] W. P. Su, J. R. Schrieffer, and A. J. Heeger, Phys. Rev. Lett. **42**, 1698 (1979).
[48] A. M. Marques and R. G. Dias, J. Phys.: Condens. Matter **30**, 305601 (2018).
[49] M. Hyrkäs, V. Apaja, and M. Manninen, Phys. Rev. A **87**, 023614 (2013).
[50] X. Li and W. V. Liu, Rep. Prog. Phys. **79**, 116401 (2016).
[51] T. Kock, C. Hippler, A. Ewerbeck, and A. Hemmerich, J. Phys. B **49**, 042001 (2016).
[52] G. Wirth, M. Ölschläger, and A. Hemmerich, Nat. Phys. **7**, 147 (2011).
[53] A. Kiely, A. Benseny, T. Busch, and A. Ruschhaupt, J. Phys. B **49**, 215003 (2016).
[54] S. Franke-Arnold, Philos. Trans. R. Soc. A **375**, 20150435 (2017).
[55] W. S. Bakr, J. I. Gillen, A. Peng, S. Fölling, and M. Greiner, Nature **462**, 74 (2009).
[56] J. F. Sherson, C. Weitenberg, M. Endres, M. Cheneau, I. Bloch, and S. Kuhr, Nature **467**, 68 (2010).
[57] M. Aidelsburger, M. Lohse, C. Schweizer, M. Atala, J. T. Barreiro, S. Nascimbène, N. R. Cooper, I. Bloch, and N. Goldman, Nat. Phys. **11**, 162 (2015).
[58] M. E. Tai, A. Lukin, M. Rispoli, R. Schittko, T. Menke, D. Borgnia, P. M. Preiss, F. Grusdt, A. M. Kaufman, and M. Greiner, Nature **546**, 519 (2017).
[59] B. K. Stuhl, H.-I. Lu, L. M. Aycock, D. Genkina, and I. B. Spielman, Science **349**, 1514 (2015).